Journal of
MATERIALS RESEARCH

Epitaxial dependence of the melting behavior of In nanoparticles embedded in Al matrices

H. W. Sheng
National Key Laboratory for RSA, Institute of Metal Research, Chinese Academy of Sciences, Shenyang 110015, People's Republic of China

G. Ren and L. M. Peng
Beijing Laboratory of Electron Microscopy, Chinese Academy of Sciences, Beijing 100080, People's Republic of China

Z. Q. Hu
National Key Laboratory for RSA, Institute of Metal Research, Chinese Academy of Sciences, Shenyang 110015, People's Republic of China

K. Lu
National Key Laboratory for RSA, and International Center for Materials Physics, Institute of Metal Research, Chinese Academy of Sciences, Shenyang 110015, People's Republic of China

(Received 19 December 1995; accepted 23 September 1996)

Nanometer-sized In particles (5–45 nm) embedded in the Al matrix were prepared by using melt-spinning and ball-milling techniques. Different crystallographic orientationships between In nanoparticles and the Al matrix were constructed by these two approaches. Melting behavior of the In particles were investigated by means of differential scanning calorimetry (DSC). It was found that the epitaxially oriented In nanoparticles (with the Al matrix) in the melt-spun sample were superheated to about 0–38 °C, whereas the randomly oriented In particles in the ball-milled sample melted below its equilibrium melting point by about 0–22 °C. We suggest that the melting temperature of In nanoparticles can be either enhanced or depressed, depending on the epitaxy between In and the Al matrix.

I. INTRODUCTION

Studies of the melting process of nanometer-sized crystallites have drawn considerable interest during recent decades, because they are not only helpful to understand the melting mechanism, but also useful to reveal the thermodynamic aspect of nanostructures. A body of evidence shows that the melting temperature of nanometer-sized free particles is often decreased, and the melting temperature depression was found to be inversely proportional to their particle sizes.[1–5] This dependence arises mainly because of the increasing surface-to-volume ratio with the decreasing particle size. Such a phenomenon has also been reported for some cases of embedded particles.[6–8] A renewed surge of experimental results shows, however, that the melting temperature for the epitaxial precipitates may also be substantially increased, as with the In and Pb embedded in an Al matrix.[9–12] Although arguments on this behavior are not in agreement, it is generally related to the interface effect. Cahn suggested that the observed superheating originates from the epitaxy between the embedded particles and the matrix, and no substantial superheating is expected for the incoherent interfaces.[13] Therefore, it is necessary to carry out a comparative study of the melting behavior of the embedded particles with different orientations with the matrix in order to clarify the intrinsic effect of the interface structures on the melting process.

II. EXPERIMENTAL

In the present work, two kinds of In nanoparticles in the Al matrix were synthesized: (i) epitaxially oriented with respect to the Al matrix in a melt-spun In/Al specimen, and (ii) randomly oriented with the Al matrix in a ball-milled specimen. A comparative investigation on their melting behavior was performed, and both superheating and melting point depression phenomena were experimentally observed.

An alloy ingot with a composition of Al–7 wt.% In was prepared by arc-melting of 99.999% pure Al and In in a water-cooled copper crucible under Ar atmosphere. The In/Al thin ribbon 2–3 mm wide, 20 μm thick, and a few meters long was obtained by the melt-spinning technique. The overall composition of the as-quenched ribbon remained as Al–7 wt.% In. Commercial elemental powder blends of Al and In (purity 99.999% and particles less than 100 mesh) with the same composition of the melt-spun sample were used as starting materi-

als for the ball-milled samples. Ball milling was performed in a vibratory ball mill. High hardness, good wear-resistant chrome steel balls were used; the ball-to-powder weight ratio was 30 : 1. The as-quenched and as-milled Al-In samples were examined by using x-ray diffraction (XRD), energy dispersive x-ray spectroscopy (EDX), transmission electron microscopy (TEM), and high resolution transmission electron microscopy (HREM) technique. XRD experiments were carried out on a Rigaku x-ray diffractometer (D/max-ra, 12 kW) with Cu K_α radiation. TEM and HREM were conducted on a JEOL-2010 microscope. Specimens for TEM and HREM observations were prepared by ion thinning for the melt-spun ribbons and for the as-milled samples (which were consolidated from the as-milled powders).

The melting behavior of In was monitored by using a Perkin-Elmer differential scanning calorimeter (DSC-7), with a sensitivity of 0.02 mJ/s for energy measurements. Either the melt-spun ribbons (5–8 pieces, about 2 mm × 2 mm × 20 μm) or the as-milled samples (compacted, about 2 mm × 2 mm × 0.5 mm) were sealed in aluminum pans and heated in a flowing argon atmosphere at a constant heating rate of 10 °C/min. The temperature with an accuracy of ±0.02 K and energy measurements for DSC were calibrated by pure In and Zn standard samples.

III. RESULTS

Figure 1(a) shows a bright-field TEM image of the In/Al melt-spun ribbon. It can be seen that the faceted In particles are distributed throughout the Al matrix. The In particle sizes are in a range of 5–40 nm with a mean diameter of 21 nm. The inset of Fig. 1(a) is the corresponding selected area electron diffraction pattern (SAED). The orientational relationship between In and Al, as well as the In cross-sectional shapes, may be obtained by tilting the matrix to different symmetric zone axes and generating the superimposed Al and In electron diffraction patterns. The In particles were found to have an orientation relationship with the Al matrix which can be described as $\{111\}_{Al} \| \{111\}_{In}$ and $\langle 110\rangle_{Al} \| \langle 110\rangle_{In}$. The In particles were also found to be truncated octahedral bounded by $\{111\}_{Al}$ and $\{100\}_{Al}$ facets (see, for details, Refs. 11 and 15). A HREM image, as shown in Fig. 1(b), shows a typical example of the hexagonal cross section of the In particles, obtained with the electron beam parallel to the $\langle 001\rangle_{Al}$ zone axis. In addition, moiré fringes and the highly ordered In/Al interfaces in the HREM image are clearly seen, suggesting the epitaxy relationship between In particles and the Al matrix. These results agree with those reported previously.[9–11] It was also found that there are some larger irregular In particles located at the Al grain boundaries.

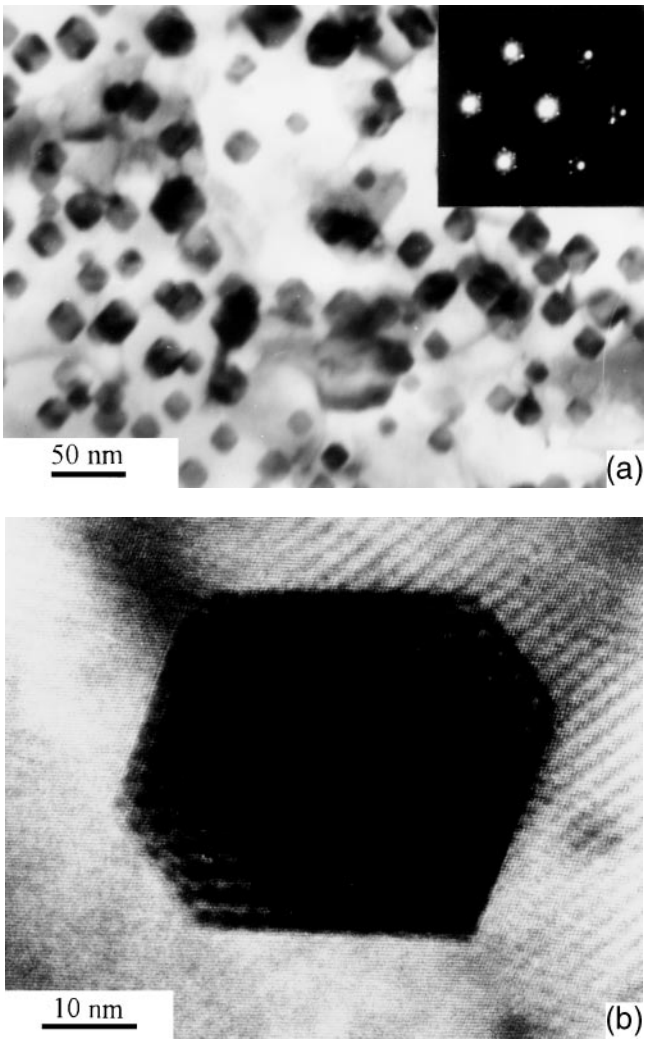

FIG. 1. (a) A typical bright-field transmission electron micrograph of melt-spun Al–7 wt.% In. Inset is the corresponding SAED, with beam direction parallel to the $\langle 110\rangle_{Al}$ zone axis. (b) A HREM observation showing the In particles epitaxially oriented with the Al matrix.

In the ball-milling experiments, we found that In particle size decreases with the milling proceeding and tends into the nanometer regime. The final product is a nanostructured mixture of pure Al and In phases. No alloying effect was observed between Al and In even when the grains are extremely small. The details of the structural changes during ball milling were reported elsewhere.[14]

A typical TEM image of the In/Al sample ball milled for 10 h was shown in Fig. 2(a). It is evident that the In particles, which are in the form of irregular shapes, are embedded in the Al matrix. The In nanoparticles, about 5–45 nm in diameter, were uniformly distributed in the Al matrix, with a statistical mean diameter of 13 nm, which is in satisfactory agreement with the XRD measurements. The inset in Fig. 2(a) is a selected area

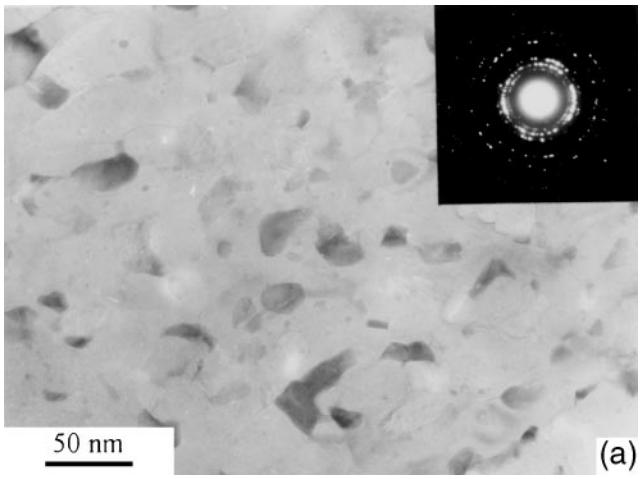

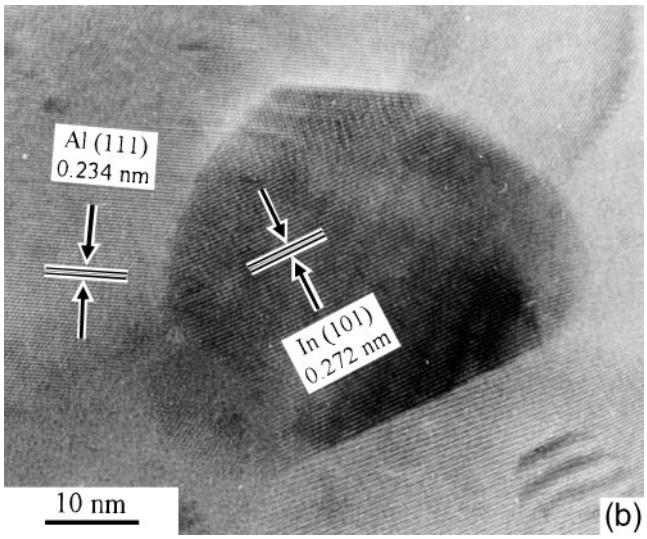

FIG. 2. (a) A bright-field TEM of ball-milled Al–7 wt.% In, and the inset is the corresponding SAED. (b) A HREM showing the morphology of the In particles and the incoherent In/Al interface.

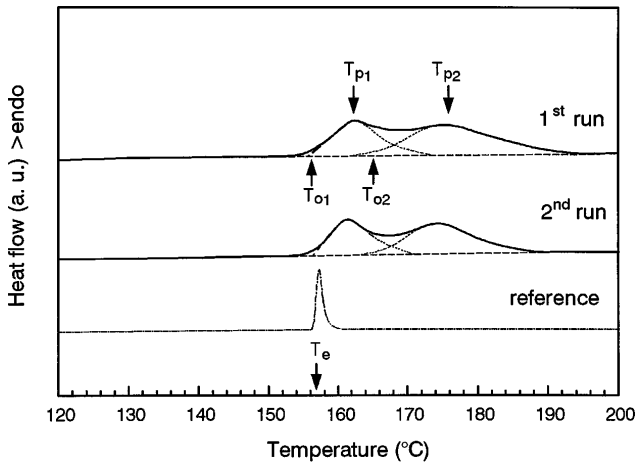

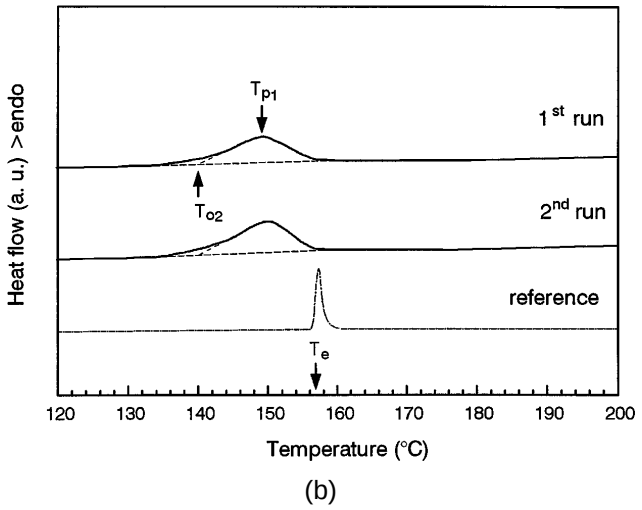

FIG. 3. DSC traces of melting endotherms for the In particles in (a) the melt-spun Al–7 wt.% In sample and (b) the ball-milled Al–7 wt.% In sample, at a heating rate of 10 °C/min. Characteristic temperatures for melting (T_o and T_p) are illustrated in the DSC curves. The reference curve is the melting DSC curve for the "bulk" In in the as-cast In/Al alloy. T_e is the equilibrium melting temperature of pure In.

electron diffraction pattern for the In/Al sample, from which we found both the In and the Al phases are random in orientations. No epitaxial orientation relationship between In and Al can be identified. HREM observations of In/Al milled powder have been performed in order to explore the morphologies of embedded In particles, and a typical HREM image is shown in Fig. 2(b). Nanometer-sized In particles are clearly found to locate either inside Al grains or at the Al grain boundaries. Interlayer phases between In/Al have not been found in our HREM observations. Evidently, morphologies and the In and Al interface structures in the as-milled sample are different from those in the melt-spun sample.

Figures 3(a) and 3(b) show typical DSC curves of endotherms for the In nanoparticles melting in the melt-spun and ball-milled Al–7 wt.% In specimens, respectively. For the melt-spun In/Al specimen [Fig. 3(a)], the In particles melted with two continuous endotherms over a temperature range of 155.9–194.0 °C. Characteristic temperatures of the two deconvoluted peaks appearing on the DSC curves are summarized in Table I. After the sample was heated up to 200 °C, and cooled down to 100 °C, a second DSC run of the same sample was performed. No substantial change in the DSC curve was found. The results are similar to those reported by Zhang and Cantor.[11] For comparison, Fig. 3 also gives the reference curves of melting of the "bulk" In (micrometer-sized) in the as-cast In/Al sample. These two endotherms might result from the melting of the irregular In particles at the Al grain boundaries and the faceted In particles within the Al grains, respectively. The *in situ* heating TEM experiments confirmed that the ultrafine In particles (5–40 nm) in the as-quenched In/Al

TABLE I. The onset and peak temperatures of melting of In in the In/Al sample under different conditions. The change in the melting point with respect to the onset of the melting of the "bulk" In in as-cast In/Al, $\Delta T = T_o - T_m$, is also shown.

		Peak 1			Peak 2		
Sample		T_{a1} (°C)	T_{p1} (°C)	ΔT (°C)	T_{o2} (°C)	T_{p2} (°C)	ΔT (°C)
Melt spun	1st	155.9	163.0	− 0.3	165.2	175.8	+ 9.0
(5–40 nm)	2nd	156.2	161.5	0	166.8	174.3	+10.6
Ball-milled	1st	139.0	149.1	−17.2	...	...	...
(5–45 nm)	2nd	139.7	152.4	−16.5	...	...	...
As cast (Ref.)		156.0	156.7	0	...	...	...

sample melt at temperatures far above the equilibrium melting point of In (by about 0–38 °C),[15] which agrees well with the broad endothermal peaks in the DSC curve.

Figure 3(b) shows the DSC curves of the In/Al powders milled for 40 h. A flat endothermal peak corresponding to the melting of In particles appears in the DSC curve. The endotherm peak spans over a wide temperature range (134.2 °C–158.0 °C), with an onset temperature of 139.0 °C. Compared with the melting peak of the reference bulk In sample, it is easy to discern that the melting temperature of the irregular nanometer-sized In particles in the Al matrix is depressed. A second run of the same sample after cooling down from 200 °C does not show any change in the shape of the endothermal peak, indicating no substantial particle coarsening takes place up to 200 °C. The melting point depression of the In particles in the Al matrix is well reproducible. The characteristic temperatures for the melting endothermal peak are listed in Table I. Similar melting behavior for Pb nanoparticles embedded in Pb/Al systems has also been detected.[16]

Due to the different synthesis processes, some additional factors may affect the melting behavior of the In nanoparticles, such as introduced impurities (in the ball-milled samples, we detected traces of iron impurities from contamination, about 0.03 wt. % per hour) and microstrains during milling and quenching processes. However, these external factors from the synthesis methods cannot account for the change in the melting behavior of In particles in the In/Al dispersions.[15]

The intrinsic mechanism for superheating is still controversial. It has been related to strain energy effects,[17,18] interface energy effects,[10,16,19] and kinetic barriers to nucleation.[11,20,21] The strain energy effects, resulting from coefficients of thermal expansion and volume expansion due to melting, may possibly cause the melting point elevation of In particles in the melt-spun sample. Compared with the observed melting point elevation of In particles, however, the elevation due to strain energy effects (about 6.2 K) is so small that it can be neglected.[15,17] In the ball-milled In/Al sample, the melting point of In will not be influenced by the strain energy effects because of the rapid relaxation of the Al matrix.[15] In one word, the strain energy effects could not explain the different melting behavior of In nanoparticles in the Al matrices.

From the thermodynamics point of view, the different melting behavior of finite particles can be related to the Gibbs–Thompson effect or interface energy effects, which have been addressed in recent papers.[10,15,16] In this paper, the different melting behavior of In particles will be alternatively interpreted according to the thermal vibration instability model,[22] which is based on Lindemann's criterion for the melting temperature[23] as described by the following equation:

$$\frac{T_m(r)}{T_m(\infty)} = \exp[-(\alpha - 1)(r/3h - 1)^{-1}],$$

where $T_m(\infty)$ is the bulk melting temperature, $T_m(r)$ is the melting temperature of a spherical particle with a radius of r, and h corresponds approximately to the height of a monolayer of atoms on the bulk crystals. α is a directly experimentally measurable parameter, which is equal to σ_s^2/σ_v^2. σ_s^2 and σ_v^2 represent the mean-square displacement for the surface and interior atoms of the corresponding crystal. It can be seen that if α is greater than 1, i.e., the surface (interface) atoms are constrained to smaller vibrations than the interior atoms, then superheating will be observed. On the other hand, intensification of thermal vibrations of the surface (interface) atoms will cause melting point depression of the embedded particles.

IV. CONCLUSIONS

For In nanoparticle in the melt-spun In/Al specimen, we observed epitaxy between In and Al. Therefore, the thermal vibration of interfacial atoms of In particles might be suppressed due to the epitaxy, as suggested by Shi,[22] leading to the parameter $\alpha < 1$, which might explain the significant superheating of In nanoparticles in the melt-spun In/Al specimen. In contrast with the epitaxy between In and Al in melt-spun In/Al, In particles are randomly oriented with the Al matrix in the ball-milled In/Al. These interfaces provide enough space for the In atoms to vibrate more freely than those atoms within the ordered In crystals. Hence, a depression of the melting temperature results, as indicated by the equation

above. Consequently, it can be concluded that the In particles in the Al matrix can be either increased or decreased, depending on the interfacial structure between In and Al.

ACKNOWLEDGMENTS

Financial support from the Chinese Academy of Sciences and the National Science Foundation of China (Grant No. 59321001) is acknowledged.

REFERENCES

1. C. R. M. Wronski, J. Appl. Phys. **18**, 1730 (1967).
2. Ph. Buffat and J-P. Borel, Phys. Rev. A **13**, 2287 (1976), and references therein.
3. L. L. Boyer, Phase Trans. **5**, 1 (1985), and references therein.
4. G. L. Allen, R. A. Bayles, W. W. Gile, and W. A. Jesser, Thin Solid Films **144**, 297 (1986).
5. T. Ben David, Y. Lereah, G. Deutscher, R. Koffman, and P. Cheyssac, Philos. Mag. A **71**, 1135 (1995).
6. K. Uenishi, H. Kawaguchi, and K. F. Kobayashi, J. Mater. Sci. **29**, 4860 (1994).
7. K. M. Unruh, J. F. Sheehan, T. E. Huber, and C. A. Huber, Nanostr. Mater. **3**, 425 (1993).
8. T. Ohashi, K. Kuroda, and H. Saka, Philos. Mag. B **65**, 1041 (1992).
9. K. Sasaki and H. Saka, Philos. Mag. A **63**, 1207 (1991).
10. H. Saka, Y. Nishikawa, and T. Imura, Philos. Mag. A **57**, 895 (1988).
11. D. L. Zhang and B. Cantor, Acta Metall. Mater. **39**, 1595 (1991).
12. L. Gråbaek, J. Bohr, E. Johnson, L. Sarholt-Kristensen, and H. H. Andersen, Phys. Rev. Lett. **64**, 934 (1990).
13. R. W. Cahn, Nature (London) **323**, 668 (1986).
14. H. W. Sheng, J. Xu, X. K. Sun, K. Lu, and Z. Q. Hu, Nanostr. Mater. **5**, 417 (1995).
15. H. W. Sheng, G. Ren, L. M. Peng, Z. Q. Hu, and K. Lu, unpublished work.
16. H. W. Sheng, G. Ren, L. M. Peng, Z. Q. Hu, and K. Lu, Philos. Mag. Lett. **73**, 179 (1996).
17. G. L. Allen, W. W. Gile, and W. A. Jesser, Acta Metall. **28**, 1695 (1980).
18. A. K. Malhotra and D. C. Van Aken, Philos. Mag. A **71**, 949 (1995).
19. P. R. Couchman and W. A. Jesser, Philos. Mag. **35**, 787 (1977).
20. J. Däges, H. Gleiter, and J. H. Perepezko, Phys. Lett. **119**, 79 (1986).
21. G. D. T. Spiller, Philos. Mag. **46**, 535 (1982).
22. F. G. Shi, J. Mater. Res. **9**, 1307 (1994).
23. F. A. Lindemann, Z. Phys. **11**, 609 (1910).